Talanta 84 (2011) 531–537

Contents lists available at ScienceDirect

Talanta

journal homepage: www.elsevier.com/locate/talanta

Signal amplification for DNA detection based on the HRP-functionalized Fe_3O_4 nanoparticles

Xiao-Ya Dong, Xiao-Na Mi, Bo Wang, Jing-Juan Xu*, Hong-Yuan Chen

The Key Lab of Analytical Chemistry for Life Science (MOE), School of Chemistry and Chemical Engineering, Nanjing University, Nanjing 210093, PR China

ARTICLE INFO

Article history:
Received 15 November 2010
Received in revised form 13 January 2011
Accepted 21 January 2011
Available online 31 January 2011

Keywords:
Electrochemical sensor
Gold nanofilm
Bioconjugates
DNA biosensors

ABSTRACT

An electrochemical approach for the sensitive detection of sequence-specific DNA has been developed. Horseradish peroxidase (HRP) assembled on the Fe_3O_4 nanoparticles (NPs) were utilized as signal amplification sources. High-content HRP was adsorbed on the Fe_3O_4 NPs via layer-by-layer (LbL) technique to prepare HRP-functionalized Fe_3O_4 NPs. Signal probe and diluting probe were then immobilized on the HRP-functionalized Fe_3O_4 NPs through the bridge of Au NPs. Thereafter, the resulting DNA–Au–HRP–Fe_3O_4 (DAHF) bioconjugates were successfully anchored to the gold nanofilm (GNF) modified electrode surface for the construction of sandwich-type electrochemical DNA biosensor. The electrochemical behaviors of the prepared biosensor had been investigated by the cyclic voltammetry (CV), chronoamperometry (*i*–*t*), and electrochemical impedance spectroscopy (EIS). Under optimal conditions, the proposed strategy could detect the target DNA down to the level of 0.7 fmol with a dynamic range spanning 4 orders of magnitude and exhibited excellent discrimination to two-base mismatched DNA and non-complementary DNA sequences.

1. Introduction

The development of highly sensitive and selective DNA sensors is a challenging subject because of its great importance in various areas such as clinical diagnosis, environmental monitoring, biological research, forensic analysis and antibioterrorism [1,2]. It also offers opportunities in understanding fundamental biological processes involved in disease development and progression and in monitoring patient responses to selected therapy methods [3]. Since the conventional methods could not meet the requirements of detecting DNA at the trace level, considerable efforts have been made towards the amplification techniques for the goal.

Recently, amplification of the sample based on polymerase chain reaction had been proved as an important strategy for sensitive DNA or protein assays [4–6]. However, it required thermal cycle process and strict laboratory conditions to avoid contamination or false results. Strategies based on the amplification of signal produced by hybridization events have demonstrated especially great potential for the direct detection of small amounts of biomolecule with impressive limits of detection. Successful signal amplification strategies include applying new redox-active probes, coupling amplification-by-polymerization concepts with electrochemical detection, integrating nanomaterials to increase loading of tags, and incorporating enzyme-assisted signal amplification processes, etc. [7–19].

Among these strategies, the enzyme amplification technology had attracted special interests due to the outstanding catalytic property and biocompatible performance of enzyme. For example, amplification of electrochemical signals has been demonstrated in stem-loop capture probe system with streptavidin–biotin chimerism for the enzyme binding [13]. With streptavidin–alkaline phosphatase as reporter molecule, enzyme-amplified electrochemical biosensor was used to detect nucleic acid sequences specific of *Legionella pneumophila* [20]. Fan and co-workers reported a stem-loop probe dually labeled with biotin and digoxigenin (DIG) to bind HRP linked-anti-DIG antibody for enzymatically amplifying the electrochemical current signal [14]. However, almost all of the enzyme amplification DNA biosensors were based on hybridization target DNA with signal probe labeled biotin, followed by conjugate with streptavidin labeled enzyme. The amount of labeled enzyme was limited via ligand–receptor interaction events, which would limit the sensitivity level of detection.

Aiming at further improving the efficiency of the enzyme amplification technology, it is anticipated that if more amount of HRP could be introduced in the detection system, the sensitivity and detection limit of DNA biosensor would be enhanced significantly. Herein, we proposed a highly efficient enzyme amplification method using DNA–Au–HRP–Fe_3O_4 (DAHF) bioconjugates as amplification label to construct the sandwich-type DNA biosensor. Fe_3O_4 nanoparticles were utilized as matrix for loading a large

* Corresponding author at: The Key Lab of Analytical Chemistry for Life Science, School of Chemistry and Chemical Engineering, Nanjing University, 22 Hankou Road, Nanjing 210093, PR China. Tel.: +86 25 83597294; fax: +86 25 83597294.
E-mail address: xujj@nju.edu.cn (J.-J. Xu).

0039-9140/$ – see front matter © 2011 Elsevier B.V. All rights reserved.
doi:10.1016/j.talanta.2011.01.060

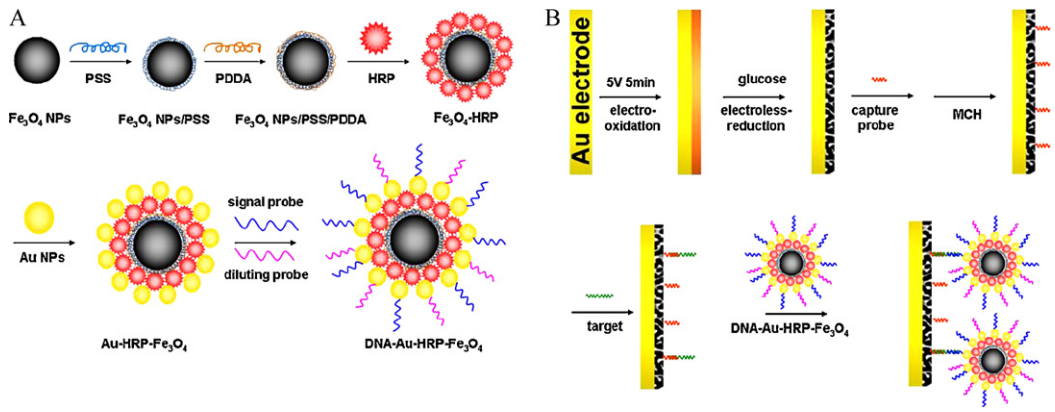

Scheme 1. Schematic for preparation of DAHF bioconjugates (A); preparation procedure of DNA sensor and the sandwich type detection strategy (B).

quantity of HRP through LbL technique, gold nanofilm (GNF) of the electrode surface with unique properties [21–25] was employed as substrate to anchor capture probe. In presence of the target DNA, hybridization would ensure the attachment of the DAHF bioconjugates onto the GNF, followed by the enzyme catalyze oxidization of TMB substrate for the amplification of electrochemical signal. Since the DAHF bioconjugates carried large quantities of HRP, the approach proposed here would provide a more sensitive method for DNA detection.

2. Experimental

2.1. Materials and reagents

Hydrogen tetrachloroaurate ($HAuCl_4$), trisodium citrate, β-d-glucose, horseradish peroxidase (HRP, MW 44,000, ~250 units/mg protein), ferric chloride hexahydrate ($FeCl_3{\bullet}6H_2O$ > 99%), ferrous chloride tetrahydrate ($FeCl_2{\bullet}4H_2O$ > 99%), sodiumdodecylsulfate (SDS), sodium hydroxide, hydrochloric acid, poly(dimethyldiallyl ammonium chloride) (PDDA), poly(sodium 4-styrenesulfonate) (PSS), tri(2-carboxyethyl) phosphinehydrochloride (TCEP), streptavidin labeled horseradish peroxidase, albumin bovine serum (BSA), 6-mercapto-1-hexanol (MCH), hexaammineruthenium(III) chloride (RuHex) were obtained from Sigma–Aldrich (St. Louis, MO). 3,3′,5,5′ tetramethylbenzidine (TMB) was purchased from Neogen (Lexington, KY) in the format of a ready-to-use reagent (K-blue low-activity substrate, H_2O_2 included). All of the synthetic oligonucleotides were purchased from Shanghai Sangong biotechnology Co. Their base sequences are as follows:

Capture probe sequence, 5′-TGG AAA ATC TCT AGC AGT CGT–$(CH_2)_6$–SH-3′.
Target DNA sequence, 5′-ACT GCT AGA GAT TTT CCA CAC TGA CTA AAA GGG TCT GAG GGA-3′.
Signal probe sequence, 5′-SH–$(CH_2)_6$–ATG TCC CTC AGA CCC TTT-3′.
Diluting probe sequence, 5′-SH–$(CH_2)_6$–GTC GCG CGA ACC GTA TAG-3′.
Two-base mismatched DNA sequences, 5′-ACT GCT AGA GAT TTT CCA CAC TGA CTA AAA GCG TCT GTG GGA-3′.
Non-complementary DNA sequences, 5′-ACT GCT AGA GAT TTT CCA CAC TGA CTA CTT CAA CAG TGC CCC-3′.
Biotinylated probe sequences, 5′-biotin–$(CH_2)_6$–ATG TCC CTC AGA CCC TTT-3′.

The other chemicals were of analytical grade and used without further purification. All aqueous solutions were prepared using ultra-pure water (Milli-Q, Millipore). The buffers involved in this work were as follows: DNA immobilization buffer, 10 mM Tris–HCl, 1.0 mM EDTA, 0.3 M NaCl, and 1.0 mM TCEP (pH 8.0); DNA hybridization buffer, 10 mM Tris–HCl, 1.0 mM EDTA, and 0.25 M NaCl (pH 8.0); Washing buffer, 10 mM phosphate buffer (PBS), 0.1% SDS and 0.1 M NaCl (pH 8.0).

2.2. Apparatus

The electrochemical measurements for cyclic voltammetry (CV), chronocoulometry (CC) and chronoamperometry (*i*–*t*) were performed on a CHI 660C electrochemical workstation (CH Instrument Co.) Electrochemical impedance spectroscopy (EIS) experiments were carried out on an Autolab PGSTAT-30 potentiostat/galvanostat (Eco Chemie BV, Utrecht, The Netherlands) with FRA software. UV–vis absorption spectra were carried out on a Shimadzu UV-3600 UV–vis–NIR photospectrometer (Shimadzu Co.) Transmission electron microscopy (TEM) images were taken with a JEOL model 2000 instrument operating at 200 kV accelerating voltage. Atomic force microscopy (AFM) images were performed in ambient conditions using a molecular imaging Pico SPM in tap mode with a 10 μm scanner.

2.3. Preparation of Au NPs and Fe_3O_4 NPs

Au NPs were prepared according to the literature [26]. Briefly, 0.6 ml of 0.1 M $NaBH_4$ was added to 20 mL aqueous solution containing 2.5×10^{-4} M $HAuCl_4$ under stirring. The solution turned to orange–red color immediately, indicating the formation of Au NPs. These particles were stirred at 25 °C for 3 h and then kept in a refrigerator at 4 °C for further use.

The Fe_3O_4 NPs were synthesized by controlled co-precipitation of Fe (II) and Fe (III) ions with 0.5 M NaOH as the reductant according to previous report [27]. Typically, 1 M $FeCl_3{\cdot}6H_2O$, 0.5 M $FeCl_2{\cdot}4H_2O$ was dissolved in 25 mL of 0.4 M HCl solution degassed with nitrogen under vigorous stirring. The co-precipitation of Fe_3O_4 NPs was carried out in a three-neck round-bottom flask. Before the co-precipitation reaction, the above mixture solution was added to 250 mL of 0.5 M NaOH, which was preheated to 80 °C. This reaction was protected under N_2 atmosphere and was vigorously stirred. Black powder was collected by sedimentation with the help of an external magnetic field and washed several times with water until stable ferro fluid was obtained. Finally, the particles were redispersed in water and stored at 4 °C.

2.4. Preparation of DAHF bioconjugates

The preparation procedure of the DAHF bioconjugates was showed in Scheme 1A. The layer-by-layer assembly of oppositely

charged PSS and PDDA was performed according to the literature [15,27] with a slight modification. The solution of Fe_3O_4 NPs (5 mg in 0.5 mL water) was added into 1 mL of PSS solution (2 mg mL^{-1}, containing 0.5 M NaCl) by 20 min sonication to obtain a homogeneous brown suspension and then standing for 20 min. The suspension was followed by centrifuging at 9000 rpm for 6 min. The supernatant was then carefully removed, and the Fe_3O_4 NPs coated with PSS (Fe_3O_4/PSS) were washed by three alternate cycles of centrifuging. Then 1 mL of PDDA solution (2 mg mL^{-1}, containing 0.5 M NaCl) was added into the Fe_3O_4/PSS suspension by 20 min sonication and standing for 20 min. Residual PDDA polymer was removed by high-speed centrifugation, and the complex was washed with water three times to obtain PDDA-functionalized Fe_3O_4 (after denoted as Fe_3O_4/PSS/PDDA). Then, Fe_3O_4/PSS/PDDA was redispersed in 2.5 mL of 10 mM pH 8.0 Tris–HCl solution. 200 μL of 10 mg/mL HRP were added to 0.5 mL of the above Fe_3O_4/PSS/PDDA solution. The reaction mixture was shaken for 30 min at 25 °C gently. After centrifugation, the obtained Fe_3O_4/PSS/PDDA/HRP were washed and dispersed in 4.0 mL of as-prepared colloidal Au NPs and stirred for overnight. Light purple Au–HRP–Fe_3O_4 conjugates were thus obtained, which were further washed with water and redispersed in 1 mL of 10 mM pH 8.0 PBS. The mixture of 15 μL of 100 μM signal probe and 60 μL of 100 μM diluting probe was added to 1 mL Au–HRP–Fe_3O_4 conjugates. After 16 h, the sodium chloride concentration was brought to 0.15 M in a stepwise manner. The formed DAHF bioconjugates were aged in salts for another 24 h and kept in a refrigerator at 4 °C. Prior to use, excess reagents were removed by magnetic separation and a dilution ratio of 1:2 with phosphate buffer was used.

2.5. Fabrication of GNF electrode

A bulk gold disk electrode was abraded with fine SiC paper, polished carefully with 0.3 and 0.05 μm alumina slurry, and then sonicated in water and absolute ethanol, respectively. The procedure for the preparation of the modified electrodes was described in our previous work [28]. Briefly, the cleaned gold electrode was first anodized under a high potential of 5 V in 0.1 M phosphate buffer (pH 7.0) for 5 min. The color of the oxidized electrode surface turned to salmon pink. Then, the electrode was dipped in 1 M β-d-glucose aqueous solution for 10 min. The color of the gold electrode surface turned to black after a few minutes and a porous gold GNF was obtained on the top of the gold electrode.

2.6. Preparation of DNA sensor based on GNF electrode

The preparation procedure of DNA sensor and the sandwich type detection strategy showed in Scheme 1B. The freshly prepared GNF was utilized for the preparation of DNA biosensor by immersing the electrode into an immobilization buffer containing 1.0 μM capture probe for 16 h. The capture probe modified electrode was further treated with 1.0 mM MCH for 1 h to obtain a well-aligned DNA monolayer, followed by washing with the washing buffer and ultra-pure water alternately to remove nonspecific adsorption. For the hybridization reaction, the electrode was immersed into 100 μL of solution containing target DNA (two-base mismatch DNA, noncomplementrary DNA) with different concentrations for a desired time at 37 °C. Next, the electrode was hybridized with DAHF bioconjugates for 3 h at room temperature. The electrode was extensively rinsed with washing buffer and dried under a stream of nitrogen prior to electrochemical characterization.

2.7. Electrochemical measurement procedure

A conventional three-electrode system involving a gold working electrode, a saturated calomel electrode (SCE), and a platinum counter electrode, was employed all through the experiment. Electrochemical impedance spectroscopy (EIS) was carried out in 50 mM $Fe(CN)_6^{3-/4-}$ solution prepared in 0.1 M KNO_3. Chronocoulometry (CC) was performed with 1.5 s of pulse period and 500 mV of pulse width in 50 μM $Ru(NH_3)_6^{3+}$. Cyclic voltammetry (CV) was carried out at a scan rate of 100 mV/s. Chronoamperometry (i–t) were performed with a fixed potential of −100 mV in 2 mL of TMB substrate. All potentials were referred to SCE, and all measurements were carried out at room temperature.

3. Results and discussion

3.1. Characterization of DAHF bioconjugates

Recent research has indicated that magnetic material can be utilized as carriers to load protein or enzyme to form bioconjugates. However, it was difficult to couple two kinds of molecules onto Fe_3O_4 NPs simultaneously for functionalization. To solve this problem, functional films on Fe_3O_4 NPs surface were developed, which used the electrostatic LbL self-assembly technique [27]. The functionalized Fe_3O_4 NPs were advantageous to the adsorption of biomolecules [29,30].

The positively charged Fe_3O_4 NPs were coated with negatively charged PSS polyelectrolyte and positively charged PDDA by electrostatic force. The assembling steps were shown in Scheme 1A. Since the isoelectric point of HRP is 7.2, it has a negatively charged surface when the pH is above 7.2. Consequently, negatively charged HRP (pH 8.0) could assemble on Fe_3O_4/PSS/PDDA. Owing to the interaction between amino groups of HRP and the Au colloid surface, the Au NPs could coated on the surface of the formed Fe_3O_4/PSS/PDDA/HRP to produce Au–HRP–Fe_3O_4 conjugates. Finally, signal probe and diluting probe functionalized with –SH was linked to the coated Au NPs through S–Au bond.

The morphology and size of Fe_3O_4 NPs, Au NPs, and Au–HRP–Fe_3O_4 conjugates were investigated by TEM in part A–C of Fig. 1, and the statistical analysis from the TEM were presented in parts D–F of Fig. 1. The average sizes of Fe_3O_4 NPs, Au NPs, and Au–HRP–Fe_3O_4 conjugates were 10 nm, 5 nm and 35 nm in diameter with a size distribution standard deviation of 1.0 nm, 1.1 nm and 1.9 nm, respectively. This dramatic increase of the size of the coated Fe_3O_4 NPs provided a strong evidence for the LbL assembly process. Compared with Au/Fe_3O_4 composites in our previous work [31], the DAHF bioconjugates showed well-defined morphology and good dispersity. That was because further diluting polyelectrolyte and increasing ultrasonic time in the preparation process enhanced the dispersion of DAHF bioconjugates prominently.

To further monitor the formation of DAHF bioconjugates, we studied the UV–vis absorption spectra of the HRP, Au NPs, Fe_3O_4 NPs and DAHF bioconjugates, respectively (Fig. 2). The appearance of the absorption peaks at 398 nm and 525 nm corresponded to the pure HRP and the Au NPs respectively, while the two absorption peaks at 400 nm and 550 nm corresponded to Au–HRP–Fe_3O_4 conjugates. The peak at 400 nm was mainly ascribed to HRP molecules, while the peak at 550 nm should be the absorption of Au NPs. Compared with pure HRP solution and pure Au NPs, the slight red shift of Au–HRP–Fe_3O_4 conjugates was attributed to the interaction between Au NPs and HRP molecules [32]. Thus, we concluded that HRP molecules and colloidal gold were successfully conjugated to the Fe_3O_4 NPs.

To characterize the catalytic performance of the obtained bioconjugates, its Michaelis constant (K_m) and the Maximum reaction velocity (V_{max}) were estimated by photometry according to the method of Hamilton et al. [33]. Based on the Lineweaver Burke plot, the values of K_m and V_{max} were found to be 0.239 mM and 3.16×10^{-3} mM s^{-1}, respectively. The value of K_m of bioconju-

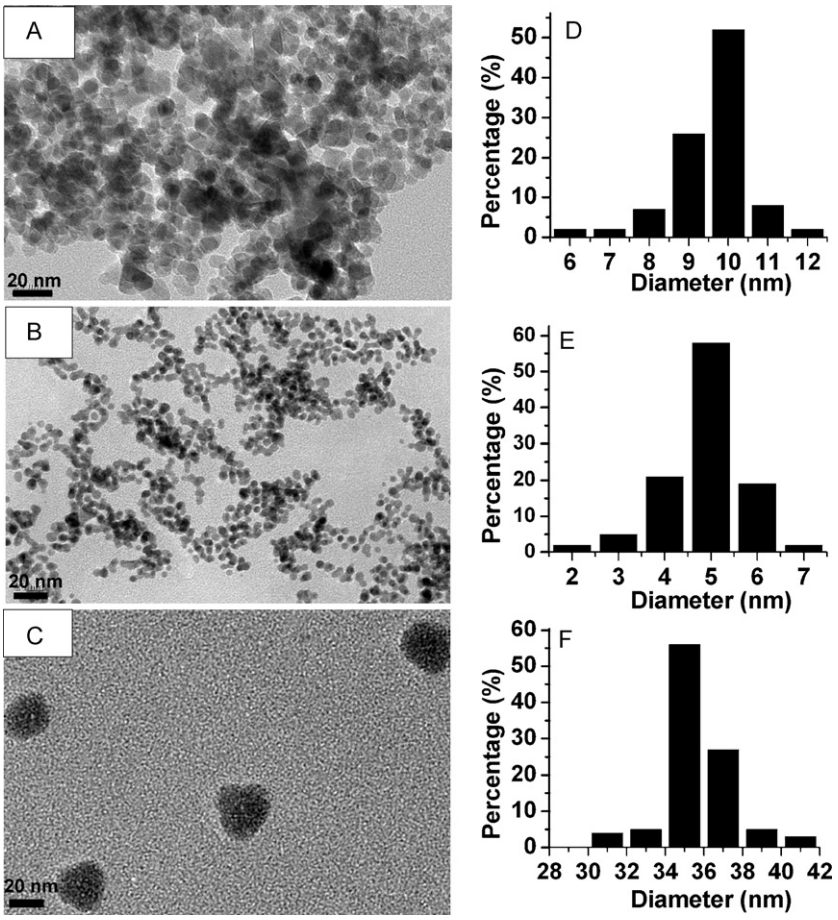

Fig. 1. TEM images of Fe_3O_4 NPs (A); Au NPs (B); Au–HRP–Fe_3O_4 conjugates (C); the size distribution of Fe_3O_4 NPs (D); Au NPs (E); Au–HRP–Fe_3O_4 conjugates (F).

gates was equal to that of 0.234 mM for free HRP, suggesting that the affinity to o-phenylenediamine is similar. The value of V_{max} was slightly lower than that of 3.31×10^{-3} mM s^{-1} for free HRP, caused by relaxation effects of HRP covered by the Au NPs.

3.2. Characterization of the GNF-based electrode

Surface condition of electrodes has an important influence on the electrochemical biosensors. Porous gold film has been highly focused owing to its unique properties. Traditional methods for preparing macroporous electrodes were based on colloidal crystal template [21–25]. Although the signal of them was higher than that of bare flat film, corrosive acid needed to be applied to eliminate the crystal template which is complicated and time-consuming. In our previous work we have reported an extremely simple and rapid approach to obtain GNF via electrooxidization of the gold surface followed by the chemical reduction of the produced gold oxide layer [28]. This process was environmentally friendly using nontoxic and inexpensive agent of β-d-glucose.

Cyclic voltammetry (CV) in 0.1 M in 0.5 M H_2SO_4 was employed to investigate the process of synthesizing the gold nanofilm (see Fig. 3). For comparison, the electrochemical responses of bare gold electrode were also shown. Typical oxidative and reductive peaks corresponding to the electrochemical behavior of Au could be observed clearly in cyclic voltammograms. The GNF electrode (Fig. 3b) had a significant larger oxidative and reductive currents than that of the bare flat electrode (Fig. 3a), indicating that the GNF electrode had a larger real area due to the formed gold nanofilm. Provided that a specific charge of 386 μC/cm^2 was required for gold oxide reduction [34], the effective area of the GNF electrode was 331.1 mm^2, while the bare flat gold electrode was 21.7 mm^2. The effective area of the GNF electrode was 15.3-fold that of the bare flat electrode. This implied that the GNF electrode was a three-dimensional structure in favor of immobilization of the capture probe.

We have investigated the morphology of the electrode with AFM (Fig. 4). The bare gold slide was smooth with roughness less than 5 nm. The electrochemical oxidation process increased the roughness of gold surface with a thickness of 100 nm. The greatly

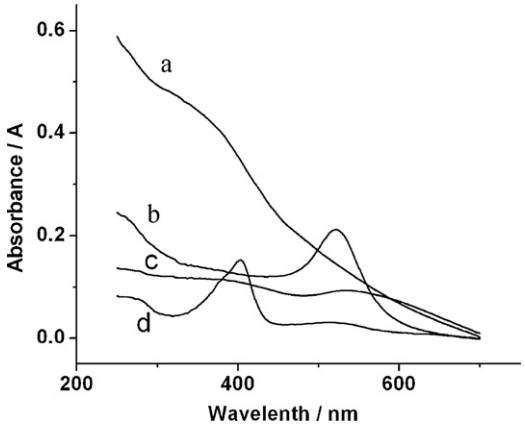

Fig. 2. UV–vis spectra of Fe_3O_4 NPs (a), Au NPs (b), Au–HRP–Fe_3O_4 conjugates (c), and HRP (d).

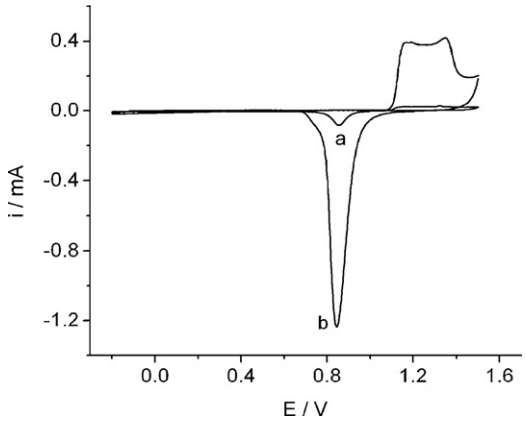

Fig. 3. Cyclic voltammograms of the bare flat Au electrode (a) and the GNF electrode (b) in 0.5 M H_2SO_4. Scan rate employed was 100 mV/s.

enhanced roughness indicated that the GNF electrode had a three-dimensional structure, which was in good agreement with the CV result mentioned above. In the presence of target DNA, the DAHF bioconjugates were linked to the GNF, and the roughness of surface increased slightly.

The assembly of oligonucleotides on electrodes and the formation of double-stranded DNA on the substrate can be followed by faradic impedance spectroscopy. Nyquist plot of impedance for the stepwise modification process with the bare flat Au electrode and the GNF electrode were investigated in Fig. 5. The equivalent circuit was shown in Fig. 5 (inset). The charge transfer resistance (R_{ct}) and the diffusion impedance (Z_w) are both in parallel to the interfacial capacitance (C_{dl}). The diameter of the semicircle corresponds to the interfacial electron-transfer resistance (R_{ct}) [35]. The increase in the diameter of the semicircle reflects the increase in the interfacial charge-transfer resistance. For the bare flat Au electrode (Fig. 5A.), the value of R_{ct} was 7.5 Ω, revealing a very small semicircle domain. After immobilization of capture probe, the value of R_{ct} increased from 7.5 to 787.5 Ω. The increase in R_{ct} was because of the negative charge of the phosphate group on the capture probe electrostatically repelled the negatively charged redox probe $[Fe(CN)_6]^{3-/4-}$ and inhibited interfacial charge transfer. Subsequently, the target DNA was hybridized with capture probe, and the R_{ct} increased again. After hybridization with DAHF bioconjugates, the value of R_{ct} increased to 1540.2 Ω. This great enhancement should be ascribed to the large size of bioconjugates which would inhibit the approach of redox probe molecules to electrode surface. In contrast, each assembling steps on the GNF electrode exhibited the similar increasing trend to that of the bare flat Au electrode. However, the R_{ct} values in each step reduced significantly. (in Fig. 5B) This fact indicated that the redox probe molecules approach GNF electrode easily for nanostructure of the GNF.

3.3. Optimization of the experiment conditions

Chronocoulometric (CC) analysis in 50 μM $Ru(NH_3)_6^{3+}$ containing 10 mM Tris–HCl (pH 7.4) at a pulse period of 1.5 s and a pulse width of 500 mV [36] was utilized to determine the density of the self-assembled capture probe on the electrode surface (Fig. 6). We measured the redox charges of $Ru(NH_3)_6^{3+}$, which was associated

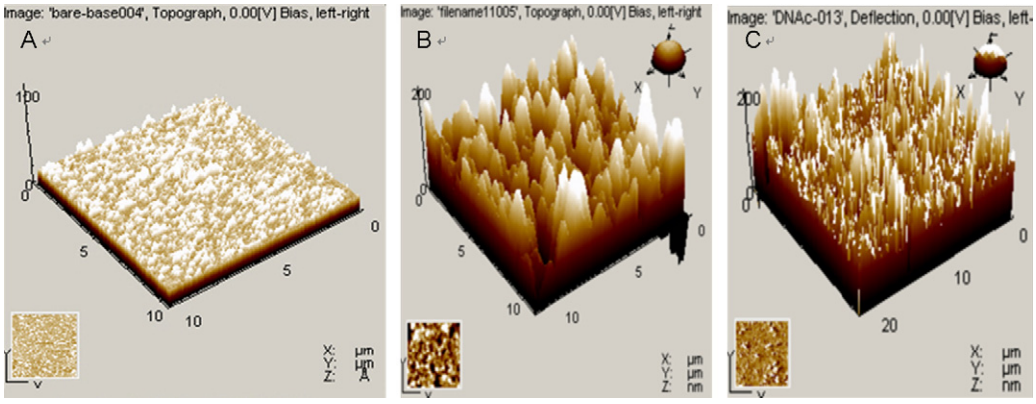

Fig. 4. AFM images of bare gold substrate (A); GNF (B); DAHF bioconjugates modified GNF(C).

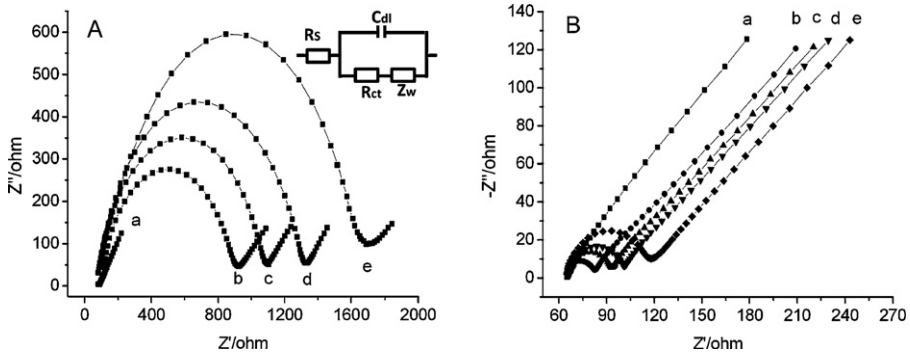

Fig. 5. Nyquist plots corresponding to flat Au electrode (A) and GNF electrode (B). (a) The bare electrode, (b) after immobilization of probe 1, (c) after immobilization probe 1 and MCH, (d) hybridization with target DNA, and (e) hybridization with the DAHF bioconjugates. The data were recorded in the presence of 50 mM $[Fe(CN)_6]^{3-/4-}$ containing 0.1 M KNO_3 as redox probe, and upon application of the biasing potential of 0.21 V, applying 5 mV alternative voltage in the frequency range of 50 mHz–10 kHz. The inset shows the equivalent circuit applied to fit the impedance spectroscopy.

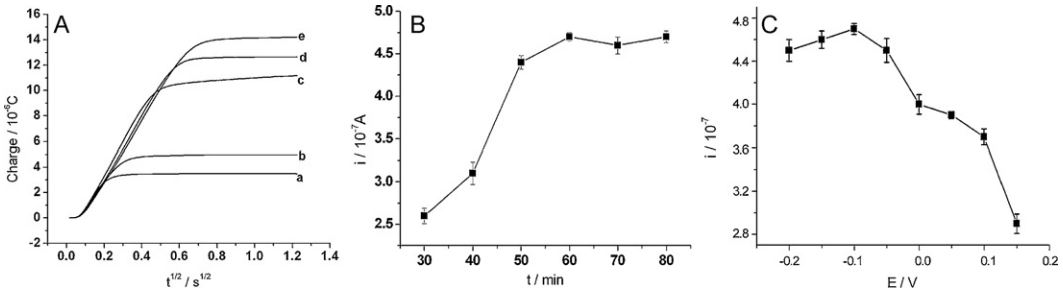

Fig. 6. (A) Chronocoulometric response curves for 1.0 μM of capture probe modified electrode in the absence of $Ru(NH_3)_6^{3+}$ (a), and 0.1 μM (b), 0.5 μM (c), 1.0 μM (d), 2.0 μM (e) of capture probe-modified electrode in the presence of 50 μM $Ru(NH_3)_6^{3+}$. (B) Effects of hybridization time on chronoamperometric responses to 1 nM target DNA; (C) effects of the applied potential on the chronoamperometric response to 1 nM target DNA. Error bars show the standard deviations (S.D.) of measurements taken from independent experiments with three different sensors.

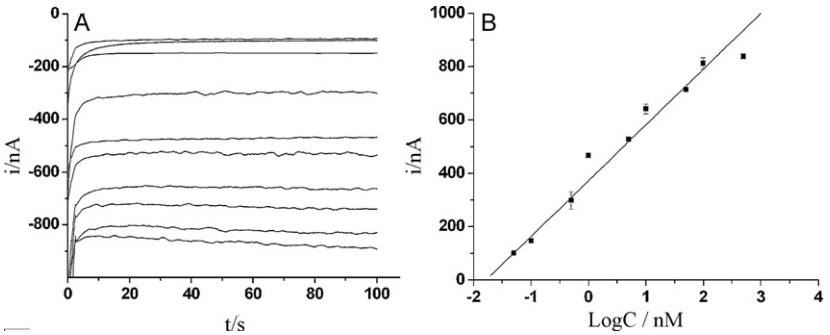

Fig. 7. (A) Chronoamperometric measurements for a range of targets DNA. From top to bottom: background, 50 pM, 100 pM, 500 pM, 1 nM, 5 nM, 10 nM, 50 nM, 100 nM, and 500 nM target DNA; (B) Plot for logarithm of the concentration of target DNA vs. chronoamperometric current with GNF electrode. Error bars represent S.D., $n = 3$.

electrostatically with the anionic DNA backbone, to estimate the surface density of the capture probe. The surface densities of capture probe with different concentrations were presented in Table 1. As the substrates modified with 0.1, 0.5, 1.0 and 10 μM capture probe, the response increased and tended to stable at 1.0 μM. Therefore, 1.0 μM capture probe was utilized in the subsequent experiments. Furthermore, surface density of the GNF electrode and bare flat gold were calculated when the concentration of capture probe was 1.0 μM. The result showed that the GNF electrode was 15.7 fold that of bare flat gold, which was coincident with the 15.3 fold enhancement of the effective surface area mentioned above. So the GNF electrode was an excellent substrate for anchoring capture probe.

When hybridizing the target DNA at 37 °C, the *i–t* responses enhanced with the increasing incubation time and then tended to a constant value after 60 min (Fig. 6B). That was because the hybridization target DNA with the capture probe reached saturation with the prolonged incubation time. Therefore, 60 min was selected as the incubation time in the sandwich-type analytical system.

The influence of the applied potential on the *i–t* signal was investigated. The maximum response showed in Fig. 6C was obtained at approximately −0.1 V (vs. SCE). At this potential, the current background was near zero and no substrate oxidation occurred. Accordingly, a working potential of −0.1 V was selected to monitor HRP activity in order to obtain highly repeatable signals.

Table 1
Calculation of the surface density on the GNF electrode surface.

Electrode	Capture probe (μM)	Surface density (molecules/cm^2)
GNF	0.1	1.36×10^{14}
GNF	0.5	2.83×10^{14}
GNF	1	3.46×10^{14}
GNF	10	3.65×10^{14}
Bare flat gold	1	2.20×10^{13}

3.4. Analytical performance

Under the optimized experimental conditions, the peak currents of the DNA biosensor were linearly proportional to the logarithm of target DNA concentration (Fig. 7). The linear calibration plot was constructed for target DNA in the range of 50 pM–500 nM, with a correlation coefficient of 0.997 ($n = 5$). The detection limit is 7.1 pM at a signal to noise ratio of 3. The 7.1 pM corresponds to the detection of 0.71 fmol of target in a 100 μL of sample solution. Control experiments were tested under the same conditions. The control biosensor was constructed on the bare gold electrode, then hybridized target, biotinylated probe and the commercial streptavidin labeled horseradish peroxidase step-by-step. The obtained peak currents of control biosensor was 7.0×10^{-8} A to 1 nM target DNA, which was less than 14.5% of the present biosensor (4.8×10^{-7} A to 1 nM target). Thus the proposed signal amplification system with DAHF bioconjugates was very efficient for sensitively electrochemical detection of DNA. In comparison with other metal NPs labeled DNA sensors [7–10] this biosensor utilized enzyme to amplify signal and simplify the experimental detection procedure without multiple steps including dissolving nanoparticles and anodic stripping voltammetry to quantify the deposited metal. Moreover, this method was superior to other enzyme amplification techniques and the detection limit has almost decreased 2 orders compared with the value in the literature [13,20].

In order to evaluate the selectivity of this biosensor, we investigated the sensor with 100 nM two-base mismatched DNA, 100 nM non-complementary DNA and 1 nM target DNA. In Fig. 8, the target DNA produced prominent signals, while the signals produced by 100-fold excess of two-base mismatched and non-complementary

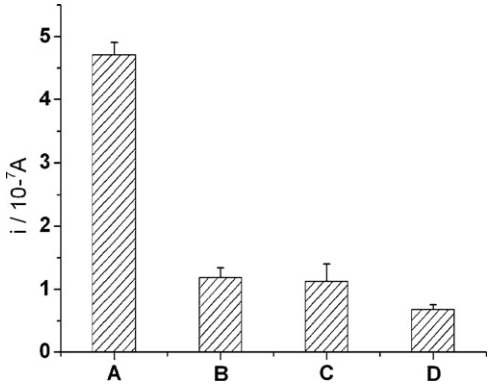

Fig. 8. Comparison of chronoamperometric signal for GNF electrodes hybridized with target DNA (1 nM) (A); two-base mismatched DNA (100 nM) (B); Non-complementary DNA (100 nM) (C); blank (D). Error bars represent S.D., $n = 3$.

DNA were not more than 12% of the target DNA. This result suggested that this sensor had excellent selectivity to target DNA.

Seven electrodes were treated in the same procedure to test the reproducibility of the method. The results showed that the relative standard deviation (RSD) was 8.4% for determination of 1 nM of target DNA under the same conditions. The stability of the biosensor was evaluated by periodically measuring the response of 1 nM target DNA. When the biosensor was kept at 4 °C, the response remained 92% of the initial signal after 1 week storage.

4. Conclusion

HRP-functionalized Fe_3O_4 NPs obtained by LbL assembly and chemisorptions technology was proposed for the construction of signal amplification platform. High-content HRP in DAHF bioconjugates coupled with the especial nanostructure of electrode surface, enabled a promising and versatile amplified platform for applications in bioanalysis. The bioconjugates as signal amplification device yielded high sensitivity, wide linear rang, low detection limit and high selectivity for detection of DNA hybridization.

Acknowledgments

This work was supported by the NSFC (grant no. 21025522, 20890021), the NSFC for Creative Research Groups (grant no. 20821063) and the 973 Program (2007CB936404).

References

[1] C. Debouck, P.N. Goodfellow, Nat. Genet. 21 (1999) 48–50.
[2] M.J. Heller, Annu. Rev. Biomed. Eng. 4 (2002) 129–153.
[3] Y. Cui, Q.Q. Wei, H.K. Park, C.M. Lieber, Science 293 (2001) 1289–1292.
[4] Y.K. Ye, J.H. Zhao, F. Yan, Y.L. Zhu, H.X. Ju, Biosens. Bioelectron. 18 (2003) 1501–1508.
[5] Z. Cheglakov, Y. Weizmann, M.K. Beissenhirtz, I. Willner, Chem. Commun. (2006) 3205–3207.
[6] P.S.C. Wu, K. Ozawa, S.P. Lim, S.G. Vasudevan, N.E. Dixon, G. Otting, Angew. Chem. Int. Ed. 46 (2007) 3356–3358.
[7] H. Cai, Y.Q. Wang, P.G. He, Y.H. Fang, Anal. Chim. Acta 469 (2002) 165–172.
[8] Z.P. Chen, Z.F. Peng, Y. Luo, B. Qu, J.H. Jiang, X.B. Zhang, G.L. Shen, R.Q. Yu, Biosens. Bioelectron. 23 (2007) 485–491.
[9] J. Wang, G.D. Liu, M.R. Jan, Q.Y. Zhu, Electrochem. Commun. 5 (2003) 1000–1004.
[10] C.F. Ding, Y. Ge, J.M. Lin, Biosens. Bioelectron. 25 (2010) 1290–1294.
[11] J. Wang, G.D. Liu, M.R. Jan, J. Am. Chem. Soc. 126 (2004) 3010–3011.
[12] S. Hwang, E. Kim, J. Kwak, Anal. Chem. 77 (2005) 579–584.
[13] X. Mao, J.H. Jiang, X.M. Xu, X. Chu, Y. Luo, G.L. Shen, R.Q. Yu, Biosens. Bioelectron. 23 (2008) 1555–1561.
[14] R.J. Cui, C. Liu, J.M. Shen, D. Gao, J.J. Zhu, H.Y. Chen, Adv. Funct. Mater. 18 (2008) 2197–2204.
[15] S. Bi, H. Zhou, S.S. Zhang, Chem. Commun. (2009) 5567–5569.
[16] B. Munge, G.D. Liu, G. Collins, J. Wang, Anal. Chem. 77 (2005) 4662–4666.
[17] R.J. Cui, H.P. Huang, Z.Z. Yin, D. Gao, J.J. Zhu, Biosens. Bioelectron. 23 (2008) 1666–1673.
[18] Y.F. Wu, C.L. Chen, S.Q. Liu, Anal. Chem. 81 (2009) 1600–1607.
[19] V. Mani, B.V. Chikkaveeraiah, V. Patel, J.S. Gutkind, J.F. Rusling, ACS Nano 3 (2009) 585–594.
[20] R. Miranda-Castro, P. De-Los-Santos-Alvarez, M.J. Lobo-Castanon, A.J. Miranda-Ordieres, P. Tunon-Blanco, Anal. Chem. 79 (2007) 4050–4055.
[21] C.H. Wang, C. Yang, Y.Y. Song, W. Gao, X.H. Xia, Adv. Funct. Mater. 15 (2005) 1267–1275.
[22] P.N. Bartlett, J.J. Baumberg, P.R. Birkin, M.A. Ghanem, M.C. Netti, Chem. Mater. 14 (2002) 2199–2208.
[23] R. Szamocki, S. Reculusa, S. Ravaine, P.N. Bartlett, A. Kuhn, R. Hempelmann, Angew. Chem. Int. Ed. 45 (2006) 1317–1321.
[24] S. Rho, D. Jahng, J.H. Lim, J. Choi, J.H. Chang, S.C. Lee, K.J. Kim, Biosens. Bioelectron. 23 (2008) 852–856.
[25] K.C. Hu, D.X. Lan, X.M. Li, S.S. Zhang, Anal. Chem. 80 (2008) 9124–9130.
[26] A. Gole, C.J. Murphy, Chem. Mater. 16 (2004) 3633–3640.
[27] S.H. Wang, X.Y. Shi, M. Van Antwerp, Z.Y. Cao, S.D. Swanson, X.D. Bi, J.R. Baker, Adv. Funct. Mater. 17 (2007) 3043–3050.
[28] W. Zhao, J.J. Xu, C.G. Shi, H.Y. Chen, Electrochem. Commun. 8 (2006) 773–778.
[29] D.Y. Wang, A.L. Rogach, F. Caruso, Nano Lett. 2 (2002) 857–861.
[30] N. Kato, F. Caruso, J. Phys. Chem. B 109 (2005) 19604–19612.
[31] Y.H. Bai, J.Y. Li, J.J. Xu, H.Y. Chen, Analyst 135 (2010) 1672–1679.
[32] D.P. Tang, J.J. Ren, Anal. Chem. 80 (2008) 8064–8070.
[33] T.M. Hamilton, A.A. Dobie-Galuska, S.M. Wietstock, J. Chem. Educ. 76 (1999) 642–644.
[34] A.J. Bard, I.R. Faulkner, Electrochemical Methods Fundamentals and Applications, Chinese ed., second ed., Beijing, Chinese version. 2001, pp. 117–117.
[35] Y. Liu, X.H. Qu, H.G. Guo, H.J. Chen, B.F. Liu, S.J. Dong, Biosens. Bioelectron. 21 (2006) 2195–2201.
[36] A.B. Steel, T.M. Herne, M.J. Tarlov, Anal. Chem. 70 (1998) 4670–4677.